

A Three Dimensional Foot Placement Planner for Locomotion in Very Rough Terrains

Ye Zhao and Luis Sentis (yezha@utexas.edu, lsentis@austin.utexas.edu)

Abstract—Maneuvering through 3D structures nimbly is pivotal to the advancement of legged locomotion. However, few methods have been developed that can generate 3D gaits in those terrains and fewer if none can be generalized to control dynamic maneuvers. In this study, foot placement planning for dynamic locomotion traversing irregular terrains is explored in three dimensional space. Given boundary values of the center of mass’ apexes during the gait, sagittal and lateral phase-plane trajectories are predicted based on multi-contact and inverted pendulum dynamics. To deal with the nonlinear dynamics of the contact motions and their dimensionality, we plan a geometric surface of motion beforehand and rely on numerical integration to solve the models. In particular, we combine multi-contact and prismatic inverted pendulum models to resolve feet transitions between steps, allowing to produce trajectory patterns similar to those observed in human locomotion. Our contributions lay in the following points: (1) the introduction of non planar surfaces to characterize the center of mass’ geometric behavior; (2) an automatic gait planner that simultaneously resolves sagittal and lateral feet placements; (3) the introduction of multi-contact dynamics to smoothly transition between steps in the rough terrains.

I. INTRODUCTION

How is it that many legged animals are capable to nimbly maneuver on 3D surfaces but humanoid robots can only slowly walk on them? To tackle this deficiency, we aim at developing new models characterizing 3D legged dynamics and designing methods to find 3D feet placements that achieve the desired gait regimes. To do so, in this paper we present a new 3D agile motion planner capable to maneuver in irregular terrains and in a natural manner. As such, this planner is aimed to control semi-autonomous legged robots in realistic outdoor environments or for the analysis of human motion.

We accomplish the 3D rough terrain capability by doing the following: (1) we develop prismatic inverted pendulum dynamics to describe the sagittal and lateral single contact behaviors, (2) we develop multi-contact models to describe the dynamics and internal forces of dual contact phases, (3) we introduce non-planar center of mass surfaces of motion to reduce the dimensionality of the model dynamics, (4) given desired feet step locations in the sagittal plane and desired apex sagittal velocities of the steps, we use numerical integration to solve sagittal feet phase placements, (5) to smoother peak velocities, we incorporate multi-contact phases and solve for the corresponding dynamics given surface friction constraints, (6) we then extract time profiles of the generated steps and use them to search lateral feet placements that keep the gait within velocity bounds, (7) we extract time profiles

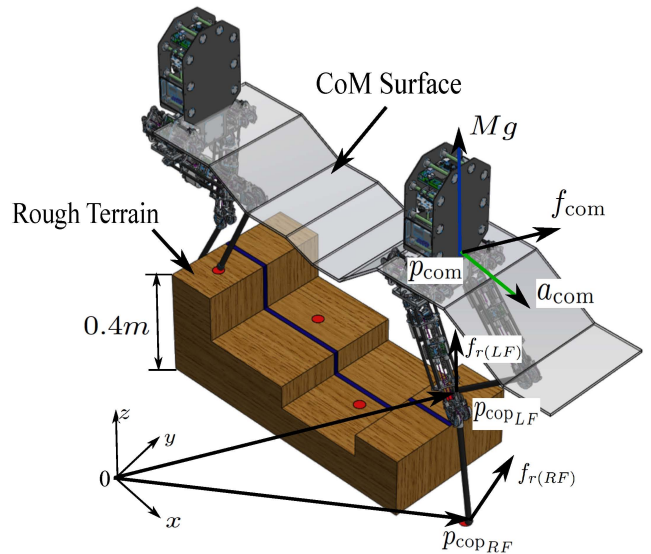


Fig. 1. **3D Schematic Diagram of Walking Profile:** The center of mass geometric surface and the feet locations on the sagittal plane are provided by the gait designer and can take arbitrary forms as long as they are kinematically feasible. The center of mass position is p_{com} , the center of pressure (CoP) positions of the right and left feet are $p_{cop(LF)}$ and $p_{cop(RF)}$. CoM accelerations are a_{com} , and reaction forces are $f_r(LF)$ and $f_r(RF)$.

of the center of mass and feet trajectories for verification and control, (8) we apply our algorithm to the terrains with irregular profiles to demonstrate the validity of our work.

One of the main characteristics of the proposed study is its generalizing principles, such as combining various contact models, relying on numerical methods, solving for feet placements in the phase plane, and maintaining center of mass movement within velocity bounds. We show the potential of our techniques in the generation of gait by maneuvering nimbly in a terrain with strong height variations using a biped visualization environment and comparing it to the performance of a human walking. To validate the applicability of our algorithm, our planner is tested on three different challenging terrains sets. Also, we have recently shown extensions of some of our methods to other gaits such as walking on vertical surfaces [1] or producing brachiation gaits [2]. Similar ideas could be used for generating gaits on quadruped robots. For instance in [3] it is shown that controlling internal tensions during rough terrain walking allows a quadruped to prevent slippage over an inclined

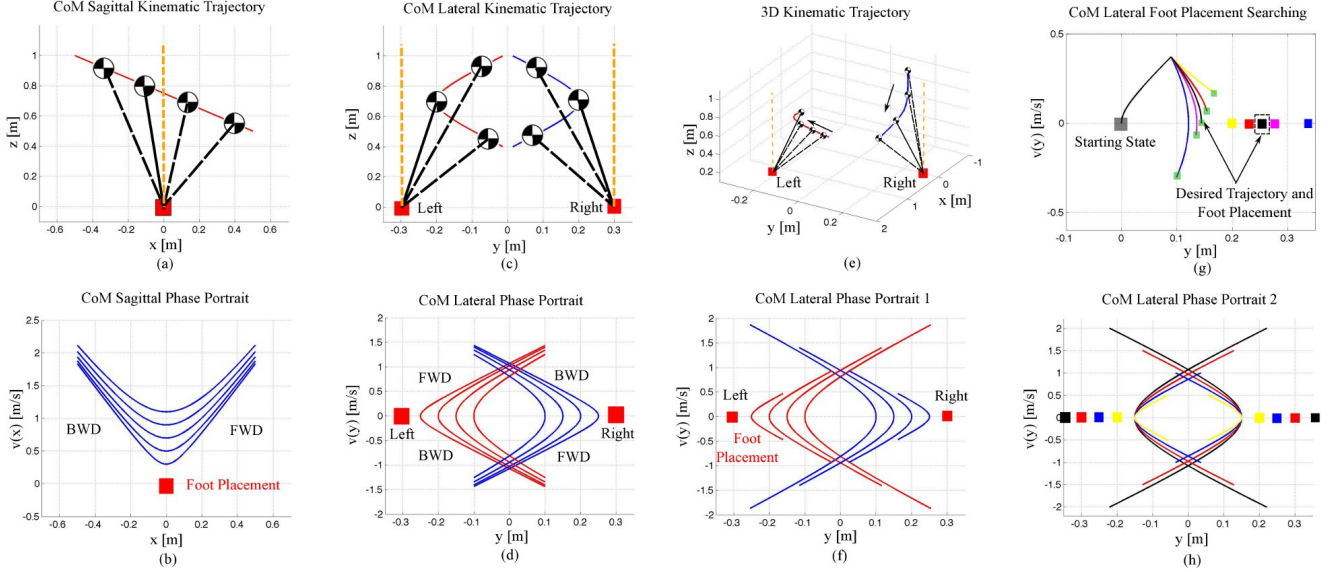


Fig. 2. **Prediction of 3D Single Contact Behaviors:** A prismatic inverted pendulum (i.e. one in which the height can change) is utilized to study the sagittal (a) and lateral (c) motion. In (a), the center of mass traverses the apex point while the center of mass in (c) bounces back before reaching the lateral foot position. The phase diagrams (b) and (d) correspond to the sagittal and lateral center of mass phase behaviors given desired feet contact locations (red boxes), a desired center of mass surface of motion, and initial position and velocity conditions. The combined 3D motion is integrated in (e). If we consider timing issues on the lateral plane as discussed in Section III, we can derive two different trajectories shown in (f) and (h). (f) shows lateral CoM behaviors given a fixed lateral foot placement and varying starting conditions. (h) corresponds to CoM trajectories derived given varying lateral foot placements and a fixed starting conditions. In (g), we analyze lateral CoM trajectories with one varying step transition.

surface.

Our work attempts to advance the state-of-the-art in rough terrain locomotion [4], [5], [6], [7], [8] and possibly help out in other works that rely on dynamic stability [9], [10], [11], [12], [13], [14]. In particular, current bipedal methods using linearized assumptions cannot achieve human like speeds in rough terrains due to the simplicity of the models, and methods relying on stability analysis require the analysis of periodic trajectories which do not apply to rough terrains. The Capture Point method described in [8] represents a powerful framework to plan feet placements. However, compared to our methods described here it only addresses gait generation in flat terrains. In contrast, our methods are applicable to non-flat 3D rough terrains because we do not utilize linearized models.

II. MATHEMATICAL DERIVATIONS

A. Decoupled 3D Prismatic Inverted Pendulums Dynamics

When considering 3D locomotion, sagittal and lateral single contact behaviors are coupled together making the foot placement generation a difficult task. However, with the assumption that the center of mass moves on a piecewise linear 3D surface, the sagittal and lateral dynamics become decoupled and therefore can be independently solved.

Using dynamic balance of moments, the difference between the moments acting on the contact foot and the net inertial and gravitational moments, is zero. Therefore, for the single contact scenario (see Figure 1) moment balance can

be written as

$$p_{\text{cop}_k} \times f_{r_k} = p_{\text{com}} \times (f_{\text{com}} + M g) + m_{\text{com}}. \quad (1)$$

where, k is the limb in contact with the ground, p_{cop_k} is the limb's center of pressure (CoP) point, f_{r_k} is the three dimensional vector of reaction forces, f_{com} and m_{com} are the three dimensional vectors of center of mass inertial forces and moments respectively, and g corresponds to the gravity field. The above equation is vectorial and determines three orthogonal moments. Force equilibrium can be formulated as $f_{r_k} = f_{\text{com}} + M g$, which allows to rewrite Equation (1) as

$$(p_{\text{com}} - p_{\text{cop}_k}) \times f_{r_k} = -m_{\text{com}}. \quad (2)$$

For our prismatic inverted pendulum model we assume single point mass [15], [16] and therefore inertial moments about the center of mass can be ignored, i.e. $m_{\text{com}} = 0$. As such, the above equation can be rewritten in vectorial form as

$$\begin{pmatrix} 0 & -f_{r_{[kz]}} & f_{r_{[ky]}} \\ f_{r_{[kz]}} & 0 & -f_{r_{[kx]}} \\ -f_{r_{[ky]}} & f_{r_{[kx]}} & 0 \end{pmatrix} \begin{pmatrix} p_{\text{com}[x]} - p_{\text{cop}_k[x]} \\ p_{\text{com}[y]} - p_{\text{cop}_k[y]} \\ p_{\text{com}[z]} - p_{\text{cop}_k[z]} \end{pmatrix} = 0. \quad (3)$$

Using the equalities $f_{r_{[kx]}} = M a_{\text{com}[x]}$, $f_{r_{[ky]}} = M a_{\text{com}[y]}$ and $f_{r_{[kz]}} = M(a_{\text{com}[z]} + g)$, we can decompose the above

equation into the following three ones

$$a_{\text{com}[x]} = \frac{\left(p_{\text{com}[x]} - p_{\text{cop}_k[x]}\right)\left(a_{\text{com}[z]} + g\right)}{p_{\text{com}[z]} - p_{\text{cop}_k[z]}}, \quad (4)$$

$$a_{\text{com}[y]} = \frac{\left(p_{\text{com}[y]} - p_{\text{cop}_k[y]}\right) \cdot a_{\text{com}[x]}}{p_{\text{com}[x]} - p_{\text{cop}_k[x]}}, \quad (5)$$

$$a_{\text{com}[z]} = \frac{\left(p_{\text{com}[z]} - p_{\text{cop}_k[z]}\right) \cdot a_{\text{com}[y]} - g}{p_{\text{com}[y]} - p_{\text{cop}_k[y]}}. \quad (6)$$

where $a_{\text{com}[\cdot]}$ represents the center of mass acceleration. We will use these three equations to formulate sagittal and lateral dynamic behavior.

B. Center of Mass Geometric Surface

Equations (4) to (6) are not only nonlinear but also multivariate and therefore they pose a problem to solve them. To deal with this difficulty we first reduce the dimensionality of the equations by planning a geometric surface of center of mass behavior beforehand. In Figure 1 we depict an example of a handmade surface. In this paper we don't explore the making of the surfaces and assume they are giving to us. In this case, the surface is piecewise linear and it approximately follows the contour of the terrain. Our surface can be expressed as

$$p_{\text{com}[z]} = \begin{cases} a_1 p_{\text{com}[x]} + b_1, & p_{\text{com}} \in \mathbb{P}_1 \\ a_2 p_{\text{com}[x]} + b_2, & p_{\text{com}} \in \mathbb{P}_2 \\ \vdots \\ a_N p_{\text{com}[x]} + b_N, & p_{\text{com}} \in \mathbb{P}_N \end{cases} \quad (7)$$

where, \mathbb{P}_i represents the path of the CoM over surface segment i . Moreover, the acceleration profile can be extracted by differentiating twice the above piecewise equation, i.e.

$$\text{if } p_{\text{com}[z]} = a_i p_{\text{com}[x]} + b_i, \text{ then } a_{\text{com}[z]} = a_i a_{\text{com}[x]}. \quad (8)$$

Let us first solve the sagittal inverted pendulum dynamics. Plugging the position and acceleration dependencies described in (8) into Equation (4) we get

$$a_{\text{com}[x]} = \frac{\left(p_{\text{com}[x]} - p_{\text{cop}_k[x]}\right)\left(a_i a_{\text{com}[x]} + g\right)}{a_i p_{\text{com}[x]} + b_i - p_{\text{cop}_k[z]}}. \quad (9)$$

and since $a_{\text{com}[x]}$ appears both on the left and right hand sides, we can rewrite the equation as

$$a_{\text{com}[x]} = \frac{\left(p_{\text{com}[x]} - p_{\text{cop}_k[x]}\right) \cdot g}{\left(a_i p_{\text{cop}_k[x]} + b_i - p_{\text{cop}_k[z]}\right)}. \quad (10)$$

The above equation represents an inverted pendulum of variable height that tracks the desired surface. Therefore we call it the prismatic inverted pendulum model and we use it to describe single contact behaviors. Notice that by defining

the center of mass surface in Figure 1, our sagittal model has now become an ordinary differential equation that can be easily solved via numerical integration.

Let us now focus on the lateral single contact dynamics. Plugging the position and acceleration dependencies of Equation (8) into (5), we get

$$a_{\text{com}[y]} = \frac{\left(p_{\text{com}[y]} - p_{\text{cop}_k[y]}\right) \cdot a_{\text{com}[z]}}{\left(p_{\text{com}[z]} - a_i p_{\text{cop}_k[x]} - b_i\right)}. \quad (11)$$

Equation (6) can be rewritten by reorganizing terms as

$$a_{\text{com}[y]} = \frac{\left(p_{\text{com}[y]} - p_{\text{cop}_k[y]}\right)}{\left(p_{\text{com}[z]} - p_{\text{cop}_k[z]}\right)} \left(a_{\text{com}[z]} + g\right).$$

Expressing $a_{\text{com}[z]}$ from (11) in terms of $a_{\text{com}[y]}$ and plugging it above we get

$$a_{\text{com}[y]} = \frac{\left(p_{\text{com}[z]} - a_i p_{\text{cop}_k[x]} - b_i\right) a_{\text{com}[y]}}{\left(p_{\text{com}[z]} - p_{\text{cop}_k[z]}\right)} + \frac{\left(p_{\text{com}[y]} - p_{\text{cop}_k[y]}\right)}{\left(p_{\text{com}[z]} - p_{\text{cop}_k[z]}\right)} g. \quad (12)$$

Isolating $a_{\text{com}[y]}$ from above, the term $a_{\text{com}[z]}$ disappears and the above equation can be written as

$$a_{\text{com}[y]} = \frac{\left(p_{\text{com}[y]} - p_{\text{cop}_k[y]}\right) \cdot g}{\left(a_i p_{\text{cop}_k[x]} + b_i - p_{\text{cop}_k[z]}\right)}. \quad (13)$$

This result is important as it represents lateral single contact dynamics as an ordinary differential equation too, and therefore independent of the dynamics of the sagittal dynamics.

C. Numerical Integration

Although we have found ordinary differential expressions that are decoupled for the sagittal and lateral planes, Equations (10) and (13) are usually nonlinear in their most general case [17]. In the special case shown in this paper it turns out that the dynamics become linear. However, considering the nonlinear case, a closed form solution of the dynamic behavior cannot be obtained. To address this limitation, we develop numerical integration techniques to solve the model dynamics.

Suppose that we have a nonlinear differential equation for the scalar variable x , and with form

$$\ddot{x} = f(x, \dot{x}). \quad (14)$$

We assume that \ddot{x} is approximately constant for small increments of time. We discretize the trajectory, (x_{k+1}, \dot{x}_{k+1}) , and derive Taylor expansions for a small disturbance, ϵ , and for initial conditions $(x_k, \dot{x}_k, \ddot{x}_k)$ to get

$$\dot{x}_{k+1} \approx \dot{x}_k + \ddot{x}_k \epsilon, \quad (15)$$

$$x_{k+1} \approx x_k + \dot{x}_k \epsilon + 0.5 \ddot{x}_k \epsilon^2. \quad (16)$$

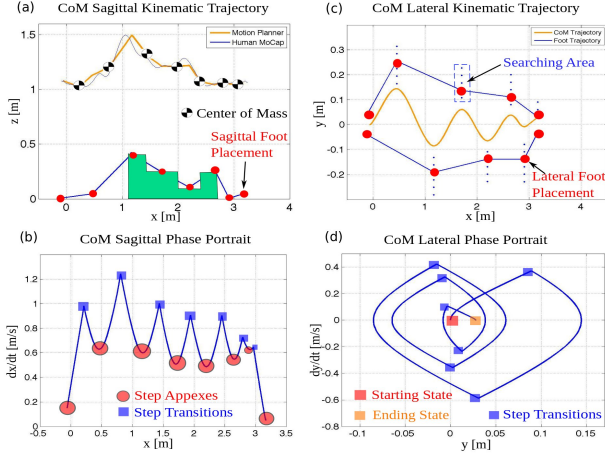


Fig. 3. **3D Automatic Motion Planner:** (a) corresponds to the user-defined geometric trajectory of the center of mass on the sagittal plane and desired sagittal foot locations, while (b) corresponds to the phase plane output of the proposed motion planner. Given step apex conditions (i.e. positions and velocities when crossing the apex), single contact dynamics generate the valley profiles shown in (b). Our planning strategy is to find intersection between adjacent contact behaviors which ensure continuity on positions and velocities. To obtain the intersections, we fit polynomials to the phase behaviors and find the roots of the polynomial resulting from subtracting adjacent curves. (d) depicts a similar strategy in the lateral plane. However, since feet transitions have already been determined in (b), what is left is to determine feet lateral positions as shown in (c). This is done so the lateral center of mass behavior shown in (d) follows a semi-periodic trajectory that is bounded within reasonable values.

From Eq. (15) we find the expression of the perturbation, $\epsilon \approx (\dot{x}_{k+1} - \dot{x}_k) / \ddot{x}_k$, and substituting in Eq. (16), with $\ddot{x}_k = f(x_k, \dot{x}_k)$, we get

$$x_{k+1} \approx \frac{(\dot{x}_{k+1}^2 - \dot{x}_k^2)}{2f(x_k, \dot{x}_k)} + x_k \quad (17)$$

which is the state-space approximate solution that we are looking for. The pipeline for finding state-space trajectories goes as follows: (1) choose a very small time perturbations ϵ , (2) given known velocities \dot{x}_k and accelerations \ddot{x}_k , and using Eq. (15), we get the next velocity \dot{x}_{k+1} , (3) using Eq. (17) we get the next position x_{k+1} , (4) plot the points (x_{k+1}, \dot{x}_{k+1}) in the phase-plane. We also notice, that we can iterate this recursion both forward and backward. If we iterate backward we then need to choose a negative perturbation ϵ .

In Figure 2, we depict various single contact scenarios of sagittal and lateral trajectories, their combined solution and the effect of changing lateral feet locations.

III. 3D MOTION PLANNING

In our previous studies [1], [17], our method successfully predicted the phase curves of center of mass sagittal behavior and was used to find the solutions of step transitions as the intersections between adjacent phase curves. See Figure 3 for a depiction of sagittal foot placements.

In this paper, our main focus is on the extension of our solver to the lateral motion plane. As such, it will allow us to create 3D gait plans. This problem is difficult because

once we have determined feet sagittal transitions, we are committed to a foot step timing. Therefore we develop a new search strategy that enables to find feet placements in the lateral plane that comply with the timing constraints.

A. Lateral Single Contact Behavior using Sagittal Timing

Similar to the sagittal case, numerical integration is used to determine phase curves. However, in the lateral case we do not know the reset condition at every step (i.e. lateral velocities at known points) since walking velocities are only specified sagittally. Instead, the main objective of lateral behavior is to produce bounded semi-periodic trajectories. Because we do not know phase plane points in the lateral plane, we rely on forward propagation of Equation (13) that complies with the timing constraints. This technique is shown in Figure 2 (g), where multiple curves are shown that complete the timing cycle of the sagittal planner but change depending on the lateral placement locations. Implementing this idea for multiple steps leads to semi-periodic gait sequences such as the one shown in Figure 3. Specifically, the blue squares correspond to the points where two curves from neighboring steps have the same position and velocity and therefore correspond to feet lateral transitions. Also, on the top right plot of the same figure we illustrate the need to search over multiple lateral locations to ensure that the trajectories are bounded.

The lateral phase portrait behaves like a semi-periodic cycle, but several differences exist resulting from the sharp contact transitions in the uneven terrain. At every step transition, a "sharp corner" appears due to the drastic change of acceleration. We will show next the need to smoother these corners by introducing multi-contact phases.

B. Search Strategy for Lateral Foot Placement

As previously shown, the 3D dynamics are broken into sagittal and lateral behavior, which are each separately solved for. However, to unify the 3D foot placement planner, the time spent during each step should be the same on both simulations. As in our previous studies [1], [17], we first solve for the sagittal feet transitions using forward and backward numerical integration and given the apex conditions (see Figure 3). Next, it is straightforward to solve for the lateral behavior using forward numerical integration and then switching contact models at exactly the same time as the feet transitions derived from the sagittal planner. The problem with this technique, is that lateral feet locations will dramatically influence the phase trajectory. If lateral feet placements are not adequately picked, the lateral behavior will not produce a bounded trajectory cycle and therefore the steps will drift away, ultimately becoming unstable.

In Equation (13) we show the direct dependencies of lateral behavior with lateral feet placements, and the plot of Figure 2 (g) shows the impact of using different placements. The question is, which foot placement is the best option? An ad-hoc choice is to choose the one that produces zero lateral velocity when the center of mass crosses the sagittal

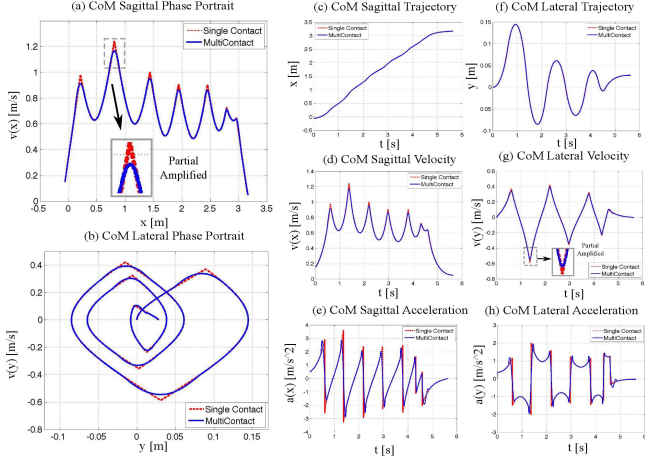


Fig. 4. **Integration of Multicontact Phases:** The plots (a) and (b) are similar to their counterparts of Figure 3 but with an addition of a multi-contact phase. A user decides the duration of the multi-contact phase with respect to the overall step and then chooses the velocity and acceleration profile during multi-contact. By using 5th order polynomials and guaranteeing continuity with the existing curves, we get the polynomial parameters and fit the curve. To determine the feasibility of the curves we extract internal forces using the multi-contact-grasp matrix presented in [1] and then determine if they are feasible given surface friction constraints. Plots (c) through (h) depict the time profiles for the sagittal and lateral trajectories.

apex of the foot. Based on this criterion, we implement a foot placement search strategy based on the Newton-Raphson bisection method, i.e.

$$(FP_y)_{k+1} = (FP_y)_k - \frac{(v_{\text{com}[y]}(\text{end}))_k}{(a_{\text{com}[y]}(\text{end}))_k} \quad (18)$$

where $(FP_y)_{k+1}$ are the candidate lateral feet placement locations for the k^{th} incremental search, $(v_{\text{com}[y]}(\text{end}))_k$ and $(a_{\text{com}[y]}(\text{end}))_k$ represent the final velocity and acceleration achieved in the previous search. For simplicity, $(a_{\text{com}[y]}(\text{end}))_k$ is obtained via numerical differentiation. The objective of the algorithm is to iterate over $(FP_y)_{k+1}$ until $(v_{\text{com}[y]}(\text{end}))_k$ is sufficiently close to zero. Overall, the search algorithm goes as follows

Algorithm 1 Newton-Raphson Search for Lateral Foot Placement

```

Assign iteration step  $k = 1$ 
Choose the initial value  $(FP_y)_1$ 
while  $k < 20$  and  $(v_{\text{com}[y]}(\text{end}))_k > 1e - 4$  do
  Implement numerical integration with  $(FP_y)_k$  for one
  step and obtain  $(v_{\text{com}[y]}(\text{end}))_k$ 
  Derive  $(FP_y)_{k+1}$  by Newton-Raphson Formula in (18)
  Implement numerical integration of  $(FP_y)_{k+1}$  for one
  step and obtain  $(v_{\text{com}[y]}(\text{end}))_{k+1}$ 
   $(a_{\text{com}[y]}(\text{end}))_{k+1} = \frac{(v_{\text{com}[y]}(\text{end}))_{k+1} - (v_{\text{com}[y]}(\text{end}))_k}{(FP_y)_{k+1} - (FP_y)_k}$ 
   $k = k + 1$ 
end while

```

The result of using the above algorithm can be seen in the

lower right plot of Figure 3.

C. Multi-Contact Transitions

Without multi-contact [1], [15], [18], contact transitions cause discontinuities in the sagittal and lateral behaviors. Moreover, such transitions are unrealistic as robots cannot switch feet instantaneously. It is also not desirable to switch feet too quickly to prevent reaching high velocity peaks (see Figure 4 (a)). Our objective here is to incorporate multi-contact transitions into our gait planner to make it look more natural and to reduce velocity peaks. For this purpose, we augment our planner with a multi-contact phase.

To incorporate a multi-contact phase, we cut out a portion of the phase curves and fit a polynomial with the desired smooth behavior. In this fitting, desired boundary values of position, velocity and acceleration are endowed by the gait designer. More importantly, it is needed to also take into account time constraints in such a way that the sagittal and lateral behaviors are exactly synchronized. Boundary and timing conditions allow us to calculate the coefficients of the polynomials.

For instance, if the polynomial of the multi-contact phase is defined by the formula

$$x(t) = \sum_{i=0}^5 a_i t^i \quad (19)$$

then we can calculate its coefficients as

$$a_0 = x_{mi}, \quad a_1 = v_{mi}, \quad a_2 = \frac{a_{mi}}{2}, \quad (20)$$

$$a_3 = \frac{1}{2t_f^3} (20x_{mf} - 20x_{mi} - (8v_{mf} + 12v_{mi})t_f - (3a_{mi} - a_{mf})t_f^2), \quad (21)$$

$$a_4 = \frac{1}{2t_f^4} (30x_{mi} - 30x_{mf} + (14v_{mf} + 16v_{mi})t_f + (3a_{mi} - 2a_{mf})t_f^2), \quad (22)$$

$$a_5 = \frac{1}{2t_f^5} (12x_{mf} - 12x_{mi} - (6v_{mf} + 6v_{mi})t_f - (a_{mi} - a_{mf})t_f^2). \quad (23)$$

where $[\cdot]_{mi}$ and $[\cdot]_{mf}$ are initial and final position, velocity and acceleration conditions, and t_i and t_f are initial and final times.

In our case, we design a multi-contact phase that takes place during 25% of the time of any given step. We show the result in Figure 4. The dotted rectangle in plot (a) of previous Figure depicts the time window for multi-contact. This percentage is adjustable to other values based on the desired walking profile. Not done here, the multi-contact profile entails internal forces that can be derived using the techniques that we proposed in [1]. The resulting internal forces would then need to be validated against the friction characteristics of the terrain.

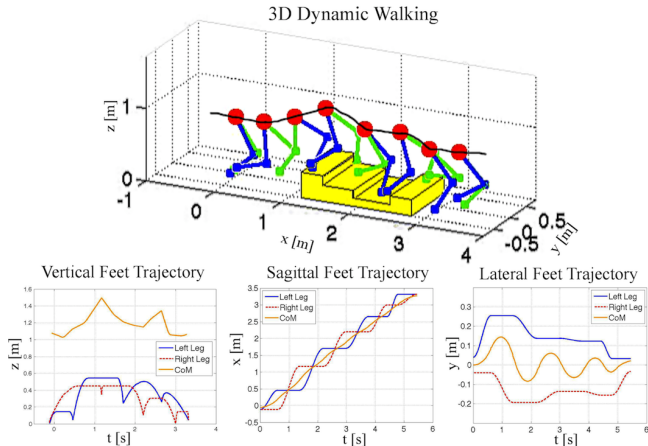


Fig. 5. **3D Dynamic Walking Animation** (a) shows an animation of the robot executing the planned trajectories. To display the results on a legged model, we fit continuous feet trajectories that converge to the desired contact conditions and we run an inverse kinematic process to obtain the resulting joint angles. Since the feet are Cartesian points we need to plan trajectories in the vertical (b), sagittal (c), and lateral axes (d).

D. Time Trajectory Generation

Our planner relies on input data sets that include: (1) the motion surface of the center of mass, (2) sagittal feet placement locations, and (3) desired sagittal velocities at the apex points. Given these data, the planner determines: (1) sagittal and lateral center of mass phase curves, (2) lateral feet locations, and (3) transition points of the feet in the phase plane. These data needs to be converted to time trajectories. Since the center of mass curves are continuous, it is straightforward to convert them into a time trajectory. On the other hand, because the feet transitions are discrete, we interpolate smooth leg swinging trajectories to land the feet at the desired time stamps. Finally, we use inverse kinematics to fit the robot’s multi-joint structure to the desired trajectories. We do this process for our case study and display it in the animation of Figure 5.

IV. MOTION CAPTURE AND CASE COMPARISON

To validate our planner we apply it to data from a motion capture process of a human maneuvering in the rough terrain. It is important to notice that data from the human is not needed for the planner to operate. Therefore it is used for validation. As shown in Figure 6, a human subject walks through a wooden rough terrain at speeds varying from 0.5 to 0.9 m/s . The experimental specifications are shown in Table 1. The gait is simultaneously captured by two cameras, one for the sagittal motion and the other one for the lateral motion. We apply scaling algorithms to compensate from perspective variations. We develop a calibration process based on comparing the data from the side and front cameras. Fourteen markers are attached to the body segments and based on the camera information, center of mass behavior is extracted.

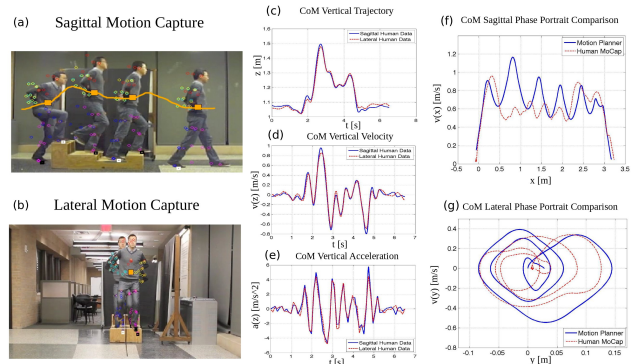


Fig. 6. **Human Walking Motion Capture:** (a) and (b) show sagittal and frontal motion data collected using two pocket cameras. In (c), (d) and (e) we compared vertical human data with the resulting trajectories from the planner. We note the good correlation of the trajectories. In (f) and (g) we superimposed the sagittal and lateral phase behaviors of the human and the planner.

In Figure 6, we compare the results between our algorithms and the data collected from the human. They correlate well with each other except for the first large step. One of the reasons might be that the human relies on ankle behavior to overcome the first obstacle. On the other hand our robot lacks an ankle and therefore needs to gain higher speed to overcome it.

TABLE I
MoCAP EXPERIMENT SPECIFICATION

| Parameter | Value | Parameter | Value |
|---|--------|-------------------|-------|
| Human Weight | 70kg | Human Height | 183cm |
| Distance between Wood Board (Right Side) and Front Camera | 7.85m | Camera Frame Rate | 25Hz |
| Wood Board Length | 1.75m | Wood Board Width | 0.7m |
| Wood Board Left Side Height | 0.45m | Walking Steps | 7 |
| Walking Speed | 0.5m/s | Walking Distance | 3.31m |

V. DYNAMIC MANEUVERING ON DIFFERENT TERRAINS

Without loss of generality, our algorithm is implemented for three more challenging terrains shown in Figure 7: inclined terrain, concave terrain and convex terrain. The walking on inclined terrain is illustrated in sequential snapshots from three different viewpoints. In this case, the height discrepancy of two consecutive stairs is specified to be a random value with a maximum of 0.2 meters. A 10 degree tilt angle is assigned to the slope of the surface. Finally, the planner generates 25 steps as shown in Figure 7 (b). Our algorithm is also tested on two different inclined terrains shown in Figure 7 (c) and (d). The average walking speed is 0.8m/s. These visualizations indicate the applicability of dynamic maneuvering on challenging terrains.

VI. DISCUSSION AND FUTURE WORK

3D legged locomotion can be solved using simple prismatic pendulum models coupled with multi-contact dynam-

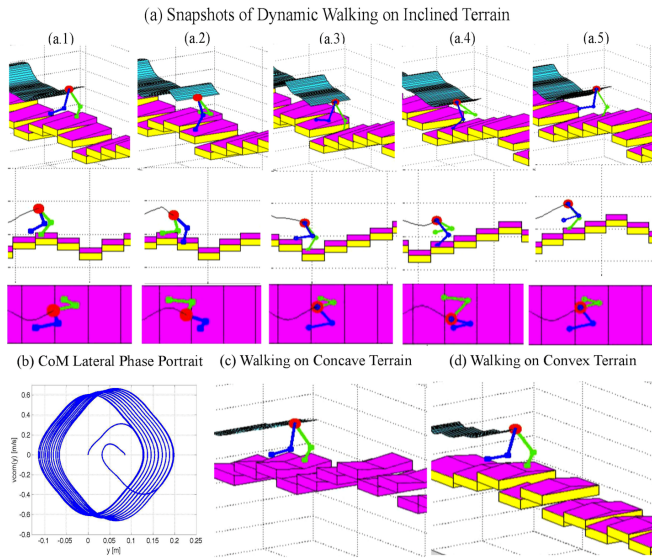


Fig. 7. **Traversing of Different Terrain Profiles:** (a) shows the snapshots of walking on a terrain with rough inclined surfaces. The side and top visualization illustrates the agile walking capabilities. The lateral CoM phase portrait in (b) shows a 25 steps walking sequence. In (c) and (d) we test the applicability of our gait generator to various terrains.

ics. To deal with the non closed-form solutions of center of mass behavior we rely on numerical integration. To reduce the dimensionality of the equations we propose to define beforehand a non-planar, piecewise linear surface of center of mass geometric behavior. This choice, results in decoupled dynamics of the sagittal and lateral phase behaviors. However, to synchronize time, we apply a Newton-Raphson search technique to determine lateral feet locations. Finally, to deal with the non-smooth transitions associated with single contact phases, we introduce multi-contact phases that comply with surface characteristics.

This paper addresses the important area of 3D gait generation in challenging terrains. In the next phase, we will focus on the design of controllers and the experimental validation of our algorithms. When the reference trajectories are applied to a real robot, modeling errors, sensor disturbances and external perturbations will cause the robot to deviate from the planned trajectories. We plan to address these issues using robust control approaches to deal with the uncertainty as well as techniques that can quickly re-plan the movement online based on realtime sensory feedback.

We also plan to develop whole-body compliant multi-contact controllers [18] to render the desired trajectories while adapting to the collisions endured with the terrain. Recently, we have implemented whole-body control algorithms in a mobile manipulator, demonstrating that it is computationally feasible [19]. Undoubtedly, much more work will be needed to implement a complete framework for legged locomotion in 3D rough terrains.

Some items to consider for future work include accounting for distributed masses and moments of inertia across the

robot's body. If distributed masses and moments of inertia are considered, dynamic coupling will be induced between sagittal and lateral motion. We plan to develop a simulated controller and run forward dynamics to estimate the moments induced by the robot. The computed moments can then be utilized to refine the gait trajectories. Additionally, during multi-contact phases, we use a fifth order polynomial to smoother the phase transitions. When using point contacts, the multi-contact dynamics have passive modes that have been ignored so far. In the future we plan to describe those dynamics and plan the transitions accordingly.

Overall, we have proposed a methodology that aims to make feasible rough terrain locomotion at human-like speeds. The overall foot placement planner is depicted in Figure 8.

VII. ACKNOWLEDGEMENTS

The authors would like to thank Mike Slovich and Kenan Isik from the HCRL at UT Austin for their help on the motion capture experiments and providing Figure's 1 drawing. We are also grateful to other HCRL members for their valuable suggestions and discussions.

REFERENCES

- [1] L. Sentis and M. Slovich, "Motion planning of extreme locomotion maneuvers using multi-contact dynamics and numerical integration," in *Humanoid Robots (Humanoids), 2011 11th IEEE-RAS International Conference on*, oct. 2011, pp. 760–767.
- [2] M. Slovich, "Case studies in multicontact locomotion (advisor: L. sentis)," Master Thesis Degree, The University of Texas at Austin, 2012.
- [3] M. Hutter, C. Remy, M. Hoepflinger, and R. Siegwart, "Scarleth: Design and control of a planar running robot," in *Intelligent Robots and Systems (IROS), 2011 IEEE/RSJ International Conference on*. IEEE, 2011, pp. 562–567.
- [4] K. Nishiwaki and S. Kagami, "Simultaneous planning of com and zmp based on the preview control method for online walking control," in *Humanoid Robots (Humanoids), 2011 11th IEEE-RAS International Conference on*. IEEE, 2011, pp. 745–751.
- [5] M. Raibert, K. Blankespoor, G. Nelson, R. Playter *et al.*, "Bigdog, the rough-terrain quadruped robot," in *Proceedings of the 17th World Congress*, 2008, pp. 10 823–10 825.
- [6] M. Kalakrishnan, J. Buchli, P. Pastor, M. Mistry, and S. Schaal, "Fast, robust quadruped locomotion over challenging terrain," in *Robotics and Automation (ICRA), 2010 IEEE International Conference on*. IEEE, 2010, pp. 2665–2670.
- [7] K. Byl and R. Tedrake, "Metastable walking machines," *The International Journal of Robotics Research*, vol. 28, no. 8, pp. 1040–1064, 2009.
- [8] J. Pratt, T. Koolen, and e. De Boer, T., "Capturability-based analysis and control of legged locomotion, part 2: Application to m2v2, a lower-body humanoid," 2012.
- [9] J. Grizzle, C. Chevallereau, A. Ames, and R. Sinnet, "3d bipedal robotic walking: models, feedback control, and open problems," in *IFAC Symposium on Nonlinear Control Systems*, 2010.
- [10] I. R. Manchester, U. Mettin, F. Iida, and R. Tedrake, "Stable dynamic walking over uneven terrain," *The International Journal of Robotics Research*, vol. 30, no. 3, pp. 265–279, 2011.
- [11] M. Hutter, C. Remy, M. Hoepflinger, and R. Siegwart, "Slip running with an articulated robotic leg," in *International Conference on Intelligent Robots and Systems*, 2010.
- [12] J. Hurst and A. Rizzi, "Physically variable compliance in running."
- [13] C. Dune, A. Herdt, O. Stasse, P. Wieber, K. Yokoi, and E. Yoshida, "Cancelling the sway motion of dynamic walking in visual servoing," in *Intelligent Robots and Systems (IROS), 2010 IEEE/RSJ International Conference on*. IEEE, 2010, pp. 3175–3180.

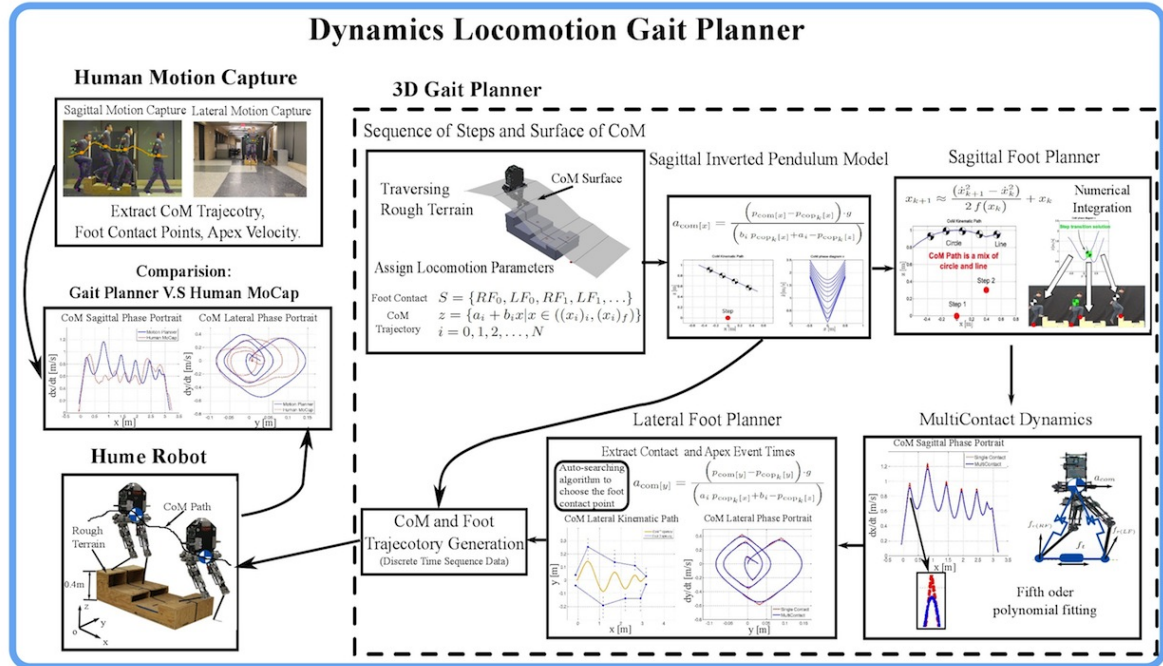


Fig. 8. **Overall 3D Foot Placement Generator.** This planner diagram depicts the sagittal foot planner (i.e. the step switching policies), the lateral foot planner (i.e. the searching strategy satisfying the timing constraint), and the multi-contact dynamics (i.e. the smoothing of the step transitions). The generated CoM and foot trajectory are extracted to be used as desired trajectory for future control purposes.

- [14] J. Engelsberger, C. Ott, M. Roa, A. Albu-Schaffer, and G. Hirzinger, "Bipedal walking control based on capture point dynamics," in *Intelligent Robots and Systems (IROS), 2011 IEEE/RSJ International Conference on*. IEEE, 2011, pp. 4420–4427.
- [15] S. Kajita, F. Kanehiro, K. Kaneko, K. Fujiwara, K. Yokoi, and H. Hirukawa, "A realtime pattern generator for biped walking," in *Robotics and Automation, 2002. Proceedings. ICRA'02. IEEE International Conference on*, vol. 1. IEEE, 2002, pp. 31–37.
- [16] S. Kajita, F. Kanehiro, K. Kaneko, K. Fujiwara, K. Harada, K. Yokoi, and H. Hirukawa, "Biped walking pattern generation by using preview control of zero-moment point," in *Robotics and Automation, 2003. Proceedings. ICRA'03. IEEE International Conference on*, vol. 2. IEEE, 2003, pp. 1620–1626.
- [17] L. Sentis and B. Fernandez, "Perturbation theory to plan dynamic locomotion in very rough terrains," in *IEEE/RSJ International Conference on Intelligent Robots and Systems*, September 2011.
- [18] L. Sentis, J. Park, and O. Khatib, "Compliant control of multi-contact and center of mass behaviors in humanoid robots," *IEEE Transactions on Robotics*, vol. 26, no. 3, pp. 483–501, June 2010.
- [19] L. Sentis, J. Petersen, and R. Philippsen, "Rough terrain whole-body manipulation," in *Autonomous Robots*, under review, 2012.